

A numerical study of the quasinormal mode excitation of Kerr black holes

Ernst Nils Dorband,^{1,2,*} Emanuele Berti,^{3,†} Peter Diener,^{1,2,‡} Erik Schnetter,^{2,§} and Manuel Tiglio^{1,2,¶}

¹*Department of Physics and Astronomy, 202 Nicholson Hall,
Louisiana State University, Baton Rouge, LA 70803, USA***

²*Center for Computation and Technology, 302 Johnston Hall,
Louisiana State University, Baton Rouge, LA 70803, USA††*

³*McDonnell Center for the Space Sciences, Department of Physics,
Washington University, St. Louis, MO 63130, USA*

We present numerical results from three-dimensional evolutions of scalar perturbations of Kerr black holes. Our simulations make use of a high-order accurate multi-block code which naturally allows for fixed adaptivity and smooth inner (excision) and outer boundaries. We focus on the quasinormal ringing phase, presenting a systematic method for extraction of the quasinormal mode frequencies and amplitudes and comparing our results against perturbation theory.

The detection of a single mode in a ringdown waveform allows for a measurement of the mass and spin of a black hole; a multimode detection would allow a test of the Kerr nature of the source. Since the possibility of a multimode detection depends on the relative mode amplitude, we study this topic in some detail. The amplitude of each mode depends exponentially on the starting time of the quasinormal regime, which is not defined unambiguously. We show that this *time-shift problem* can be circumvented by looking at appropriately chosen *relative* mode amplitudes. From our simulations we extract the quasinormal frequencies and the relative and absolute amplitudes of corotating and counterrotating modes (including overtones in the corotating case). We study the dependence of these amplitudes on the shape of the initial perturbation, the angular dependence of the mode and the black hole spin, comparing against results from perturbation theory in the so-called asymptotic approximation. We also compare the quasinormal frequencies from our numerical simulations with predictions from perturbation theory, finding excellent agreement. For rapidly rotating black holes (of spin $j = 0.98$) we can extract the quasinormal frequencies of not only the fundamental mode, but also of the first two overtones. Finally we study under what conditions the relative amplitude between given pairs of modes gets maximally excited and present a quantitative analysis of rotational mode–mode coupling. The main conclusions and techniques of our analysis are quite general and, as such, should be of interest in the study of ringdown gravitational waves produced by astrophysical gravitational wave sources.

PACS numbers: 04.30.Db, 04.70.-s, 04.80.Nn, 04.25.Dm

I. INTRODUCTION

One of the most useful methods to explore the response of black holes to external perturbations is based on wave scattering [1]. Early studies identified three main stages in the dynamics of a wave propagating on a black hole background, as observed at a fixed spatial point. In a first, transient phase the observed wave depends on the structure of the initial pulse. Vishveshwara and Press discovered that this initial “burst” is invariably followed by a second phase characterized by exponentially decaying oscillations: this phase is usually referred to as “quasinormal ringing” [2, 3]. In the third and last stage of the evolution, waves slowly die off as a power law tail [4].

Astrophysical black holes should be well described by the Kerr solution, since charge is unlikely to play a major role in astrophysical scenarios (see e.g. [5] for a discussion). As a consequence of the “no hair theorem”, if general relativity is the correct theory of gravity, the quasinormal mode (QNM) frequencies of a Kerr black hole depend only on its mass and angular momentum. Earth-based and space-based gravitational wave detectors have the potential to measure the frequency and damping time of a QNM. From these two observables we can infer the black hole’s mass

*Electronic address: dorband@cct.lsu.edu

†Electronic address: berti@wugrav.wustl.edu

‡Electronic address: diener@cct.lsu.edu

§Electronic address: schnetter@cct.lsu.edu

¶Electronic address: tiglio@cct.lsu.edu

**URL: <http://relativity.phys.lsu.edu/>

††URL: <http://www.cct.lsu.edu/>

and angular momentum [6, 7]. For the space-based *Laser Interferometer Space Antenna* (LISA), and possibly also for second-generation ground-based detectors, the signal-to-noise ratio can be large enough that we will be able to identify *two* or more QNM frequencies in the signal [8]. A multi-mode detection would provide a striking, direct test of the Kerr nature of the source (i.e., of the no-hair theorem). The basic idea is quite simple. Roughly speaking, the first mode in the pair is used to determine the black hole’s mass and angular momentum, and the other mode(s) to verify that the QNM spectrum is indeed consistent with a general relativistic Kerr black hole [9].

The combined observation of supermassive black hole binary inspiral and ringdown with LISA can provide even more information [10]. Parameter estimation during the inspiral phase can be very accurate, depending on the black holes’ masses, spins and distance [11]. Combining information from the inspiral and ringdown phases we can estimate the energy radiated in the merger, and possibly improve parameter estimation from both phases (see e.g. [12] for a preliminary study of this effect in the context of earth-based detectors).

In the last thirty years the development of gravitational wave astronomy motivated a detailed investigation of the QNM frequency spectrum [13, 14, 15]. In comparison, the problem of the *relative excitation* of QNMs received very little attention (see e.g. [16] and references therein). Ideally, the relative QNM excitation should be determined by general relativistic simulations of binary black hole mergers. Despite recent progress, this information is not yet available [17]. Given the recent progress of numerical relativity, by the time LISA flies we could have a good knowledge of the multipolar distribution of the energy and angular momentum radiated in a black hole merger under generic conditions. Knowing in advance which modes should be excited in a realistic merger will not only be useful to probe the Kerr nature of the source, but also to reduce the number of templates needed to perform matched filtering on ringdown waveforms.

In this paper we present a quantitative investigation of QNM excitation studying a simple model problem: the scattering of scalar waves on a Kerr background. We use our new infrastructure for multi-block simulations [18] for these studies. The infrastructure is based on the techniques described and applied in the context of numerical relativity in [19] and further extended in [20]. Our infrastructure uses Carpet [21, 22], a driver for the Cactus computational toolkit [23, 24], originally designed to provide fixed and adaptive mesh refinement. The capabilities of Carpet have been recently extended [18] to include the type of boundary conditions that are needed for multi-block (also called multi-patch) simulations in Cactus.

Multi-block techniques yield increased efficiency and accuracy in our studies, for two main reasons. The first is that we can set up smooth excision and outer boundaries, and we can therefore apply boundary conditions in a clean and well understood way. Furthermore, a suitable multi-block grid structure provides a natural and flexible way of implementing mesh refinement. We can keep a fixed angular resolution throughout the entire domain, avoiding the unnecessary high resolution at large distances from the central object that one would have using a cartesian grid. The resources thus saved can be used, for example, to set up a rather large number of grid points in the radial direction, so that outer boundaries are located at large radii and the noise produced at the boundaries does not affect the results. Even though we are working in three dimensions, our results are more accurate than previous studies using two-dimensional codes [25, 26]. Krivan *et al.* [25] studied the late time dynamics and the rotational coupling of massless scalar fields in a Kerr background, but not their quasinormal ringing. Later they extended the analysis to gravitational perturbations, considering both the late time tail and the quasinormal ringing phase [26]. For large rotation the damping times of corotating fundamental modes in [26] are accurate within $\sim 3\%$ when compared to results from perturbation theory; our accuracy ($\sim 0.3\%$) is roughly an order of magnitude better. In fact, we can extract the frequencies of some *overtones* with an error of the order of a few percent or less.

Given the high accuracy of our multi-block infrastructure, a careful extraction of the QNM content of the waveforms becomes necessary. We discuss in detail the so-called *time-shift problem* (exponential dependence of the quasinormal amplitudes on the time at which the quasinormal ringing regime starts), how it affects the determination of both absolute and relative QNM amplitudes, and how to choose pairs of modes so as to decrease the uncertainty on relative amplitudes. We also introduce a general criterion (based on minimizing a suitably defined residual) to determine the optimal fitting window to extract QNM frequencies and amplitudes. Using these tools we study the absolute and relative amplitudes of corotating and counterrotating modes for Gaussian initial data located in the far zone. We study the dependence of these amplitudes on the radial shape of the initial data, finding excellent agreement with results from perturbation theory [16]. We also discuss the problem of extracting overtones for modes with a given angular dependence, finding that the first overtones of corotating modes (e.g. modes with $l = m = 2$) contribute significantly to the waveform for rapidly rotating black holes.

The plan of the paper is as follows. In Sec. II we briefly describe our multi-block code. After introducing the background metric, we discuss the numerical implementation of the scalar wave equation and our time evolution techniques. In Sec. III we extract QNM frequencies and amplitudes from our evolutions, comparing with analytical predictions from perturbation theory. To start with, we point out some conceptual limitations in the extraction of QNM amplitudes due to the so-called *time-shift problem*. Then we introduce a rather general method to determine the best fitting interval to extract QNM waveforms. We first check the accuracy of this method (and of our numerical

code) by reproducing the QNM frequencies predicted by standard perturbation theory. Scalar QNM frequencies for Kerr black holes have been computed in [5], and they have never been systematically confirmed by numerical time evolutions¹. Next we give a quantitative estimate of rotational mode mixing as a function of the black hole's spin and discuss the initial data dependence of the amplitudes of corotating and counterrotating modes. In this way we assess the validity of the amplitudes predicted by perturbation theory in the so-called asymptotic approximation (where both the observer and the initial data are located far away from the black hole). Finally we discuss the extraction of overtones from our waveforms.

II. NUMERICAL EVOLUTION OF SCALAR PERTURBATIONS OF KERR BLACK HOLES

A. Grid structure

We perform our evolutions describing scalar perturbations of a Kerr spacetime through excision of the singularity. With our multi-block approach we can have smooth (in particular, spherical) inner (excision) and outer boundaries. As in [19], we use a six-block setup with a global topology of $S^2 \times R^+$, referred to as *cubed sphere* coordinates (Fig. 1). This topology and the corresponding coordinates on each block are well adapted for modeling a single central object together with outgoing radiation that is generated at or close to that object.

The six blocks are arranged like the six faces of a cube, i.e., block 0 covers the neighborhood of positive x , block 1 positive y , block 2 negative x , block 3 negative y , block 4 positive z , and block 5 negative z . On each of those blocks a local coordinate system $(\hat{a}, \hat{b}, \hat{c})$ is defined, with $-1 \leq (\hat{a}, \hat{b}, \hat{c}) \leq +1$, and equal grid spacing in the local system. The coordinate \hat{c} runs along the radial direction, and \hat{a}, \hat{b} span the angular ones. See [19] for the explicit definition of these coordinates.

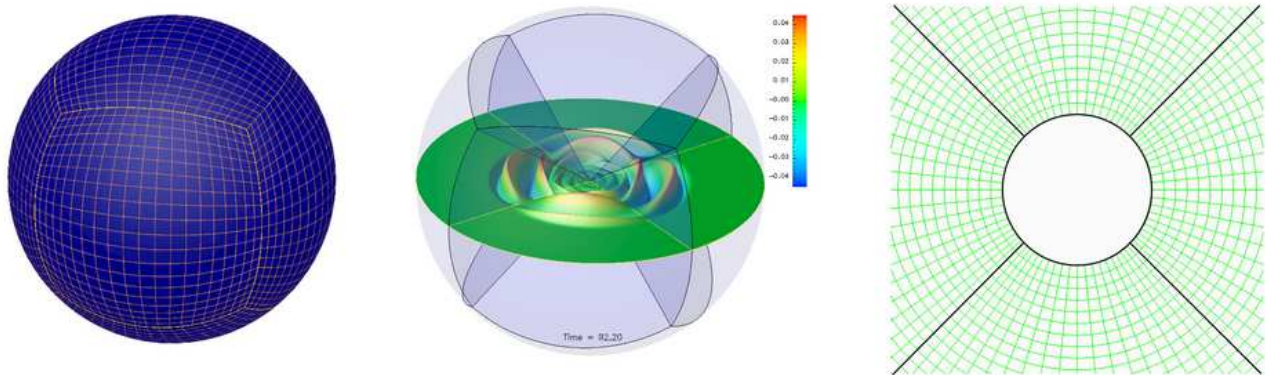


Figure 1: Illustration of the six-block grid structure and the cubed sphere coordinates that are used for the simulations in this paper. The left panel shows the distribution of grid points on a sphere of constant radius. The central panel shows a snapshot from a scalar wave evolution on an equatorial cut. The plot refers to an $\ell = m = 2$ mode on the background of a Kerr black hole with spin $j = 0.9$ at $t = 92.2M$. Also shown are the locations of the inter-block boundaries. The right panel magnifies the central region of the domain in the equatorial plane, showing the grid structure around the spherical excision boundary. The four dark lines mark the interfaces between blocks.

B. Background metric

We consider a stationary, rotating black hole background. The Kerr metric can be written in Kerr-Schild form as

$$ds^2 = \eta_{\mu\nu} + 2Hl_\mu l_\nu dx^\mu dx^\nu \quad (1)$$

¹ See however [27], where the fundamental scalar mode with $l = 0$ was observed to dominate the emission of scalar radiation by perturbed Kerr black holes in the Brans-Dicke theory of gravity.

with $\eta_{\mu\nu}$ the Minkowski metric, and

$$H = \frac{Mr}{r^2 + a^2 (z/r)^2}, \quad (2)$$

$$r^2 = \frac{1}{2}(\rho^2 - a^2) + \sqrt{\frac{1}{4}(\rho^2 - a^2)^2 + a^2 z^2}, \quad (3)$$

$$\rho^2 = x^2 + y^2 + z^2. \quad (4)$$

Here M is the mass and $a = jM = J/M$ is the angular momentum per unit mass of the black hole (j is the dimensionless spin parameter, $0 \leq j \leq 1$). In Cartesian coordinates, the null vector l_μ is given by

$$l_\mu dx^\mu = dt + \frac{rx + ay}{r^2 + a^2} dx + \frac{ry - ax}{r^2 + a^2} dy + \frac{z}{r} dz. \quad (5)$$

This form of the Kerr-Schild metric has become of common use in numerical relativity. However, in these coordinates the shape of the Cauchy and event horizons become more and more ellipsoidal with increasing spin². For $j \gtrsim 0.96$ it is not possible to fit a spherical excision boundary between these horizons any more. This is illustrated in Fig. 2. Although we could in principle choose a different shape for the excision boundary within our code, we instead use coordinates in which both horizons are always spherical, and therefore an excision sphere can always fit between them. This version of the Kerr Schild coordinates is related to the “standard” one defined above by the following transformation:

$$\tilde{x} = x - \frac{ay}{r}, \quad (6a)$$

$$\tilde{y} = y + \frac{ax}{r}, \quad (6b)$$

$$\tilde{z} = z. \quad (6c)$$

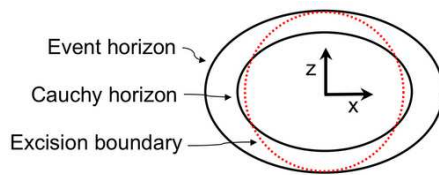


Figure 2: Event and Cauchy horizons for a Kerr black hole with spin $j \gtrsim 0.96$ in “standard” Kerr-Schild coordinates (as defined in the text), here shown in the x - z plane. The horizons have an ellipsoidal shape; it is therefore not possible to fit a spherical excision region (dotted line) between the two horizons.

C. Evolution system

We write the time evolution equations for scalar perturbations in a symmetric hyperbolic and (in the case of a stationary background) conservative form. This guarantees stability and energy conservation for the continuum equations. We use differencing operators that satisfy the summation by parts (SBP) property, and this also guarantees stability and energy conservation in the semi-discrete case (see e.g. [28] for more details). On a time independent background the evolution equations take the form

$$\dot{\Phi} = \Pi, \quad (7)$$

$$\dot{\Pi} = \beta^i \partial_i \Pi + \frac{\alpha}{\sqrt{h}} \partial_i \left(\frac{\sqrt{h}}{\alpha} \beta^i \Pi + \alpha \sqrt{h} H^{ij} d_j \right), \quad (8)$$

$$\dot{d}_i = \partial_i \Pi, \quad (9)$$

² We thank Harald Pfeiffer for pointing this out to us.

where Φ denotes the scalar field, Π its time derivative, and $d_i = \partial_i \Phi$ the spatial gradient of the field. The quantity h_{ij} is the three metric, h its determinant, h^{ij} the inverse three metric, α the lapse, and β^i the shift vector. $H^{ij} = h^{ij} - \beta^i \beta^j / \alpha^2$ is the spatial part of the inverse four-metric.

The background geometry for all simulations presented here is that of a Kerr black hole. It would be possible to exploit the axisymmetry of the background spacetime by performing a multipole decomposition of the scalar field, and then solving for each azimuthal number m as an axisymmetric, two-dimensional problem. We choose not to do so here but instead solve the full three-dimensional equations. This has the advantage that we can later use the same implementation for generic, non-axisymmetric spacetimes. Using a fully three-dimensional code also serves to test our numerical multi-block and excision techniques in a scenario that is non-trivial, but at the same time not as complicated as solving the full Einstein equations.

D. Initial and boundary conditions

The QNM excitation depends on the angular structure of the scalar field that is used as a perturbation. To excite certain modes in a controlled way, we choose initial data of the form

$$\Phi = A \exp\left(-\frac{(r-r_0)^2}{\sigma^2}\right) Y_{\ell m}, \quad (10a)$$

$$\Pi = B \exp\left(-\frac{(r-r_0)^2}{\sigma^2}\right) Y_{\ell m}, \quad (10b)$$

$$d_i = \partial_i \Phi. \quad (10c)$$

Unless otherwise stated, throughout this paper we use $r_0 = 20M$ and $\sigma = M$. $Y_{\ell m}(\theta, \phi)$ denotes the ordinary spherical harmonics. Since the Kerr background is not spherically symmetric, we should really expand the perturbation in terms of spin-weighted spheroidal harmonics ${}_s S_{\ell m}(j\omega)$ of spin weight $s = 0$. Using spherical harmonics weakly excites other modes through rotational mode mixing; this point will be discussed in more detail below, in Sec. III D.

The changes in the characteristic length scale in the radial direction are usually small over time. To accurately resolve the propagating waves all the way to the outer boundary we use a constant resolution in the radial direction of our cubed sphere coordinates. As mentioned, the coordinates are set up so that the spherical inner (excision) boundary is placed between the event and Cauchy horizons, and no boundary conditions need to be applied there. For global stability we choose maximally dissipative boundary conditions at the outer boundary, and we apply them through penalty terms.

E. Specifications for the simulations

We use spatial finite differencing operators that satisfy summation by parts; they are eighth order accurate in the interior and fourth order accurate at and close to the boundaries. With those operators we expect a global accuracy of order five (see [20] for more details on the operators that we use). We use a fourth order accurate Runge Kutta time integrator. This does not spoil the expected global fifth order spatial convergence, since we use a small enough time step so that the truncation errors generated by the time integration are smaller than those that originate from the spatial finite differencing (see [20] for details on the code's convergence).

In multi-block simulations one does not necessarily have a uniform or isotropic grid spacing in a global coordinate system. Since in all our simulations the global grid spacing in the radial direction is smaller than in the angular directions, we use the radial direction for our time step criterion $\Delta t = \lambda \Delta r$, where λ —usually referred to as the Courant factor—is chosen to be $\lambda = 0.25$.

Taking into account our initial data [cf. Eq. (10)] and the typical position of the observer, and given that we are interested in the ringdown phase, evolution times of about $t = 150M$ with outer boundaries at about $200M$ are a reasonable choice. Unless otherwise stated, for the simulations that we show below we use ten points per length unit M in the radial direction and an angular resolution of 21×21 grid points per block, which gives us approximately 80 grid points along the circumference of any sphere with constant radius. As described below, we have found that with this resolution we can get good agreement with the Kerr quasinormal frequencies predicted by perturbation theory.

Figure 3 shows a typical waveform that we get when extracting the real part of the $\ell = 2, m = 2$ mode from our simulations. The initial data are set up according to Eq. (10), with the specific choice $A = 0, B = 1, \sigma = M$ and $r_0 = 20M$. The background Kerr black hole has a spin $j = 0.9$. The strongest modes in this waveform are $(\ell = 2, m = 2, n = 0)$ and $(\ell = 2, m = -2, n = 0)$, where we use n to label overtones, $n = 0$ being the fundamental mode. We show a fit for those two modes together with the numerical data. The third strongest component in the

data is the $(\ell = 2, m = 2, n = 1)$ mode. Since this mode is decaying much faster than the fundamental mode, it only plays a role at early times. That is the reason why our fit, done for only the two fundamental modes, is drifting away from the numerical data at times below $50M$ (we will explicitly analyze overtones in Sec. III F).

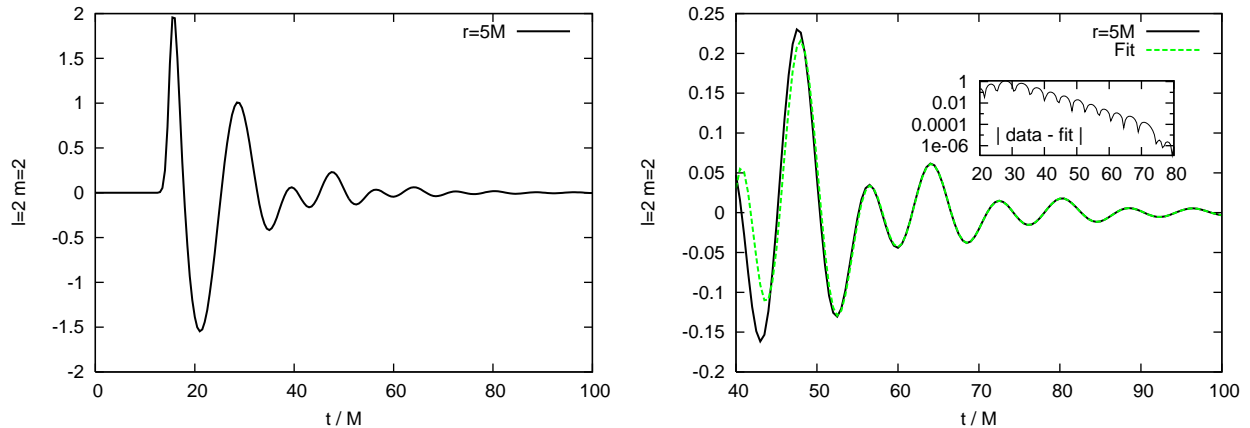


Figure 3: The left panel shows the $\ell = m = 2$ component of the waveform extracted at radius $r = 5M$ on a Kerr black hole background with a spin of $j = 0.9$. The waveform is a superposition of the corotating and the counterrotating mode, and the beating of two different frequencies is clearly visible. The right panel shows the waveform for $t \geq 40M$ as well as a QNM fit with the fundamental $\ell = |m| = 2$ modes. The interval used for the fit is $[74.5M, 150M]$. The inlay shows the absolute value of the difference between the fit and the data. At times between the excitation of the QNM ($t \sim 25M$) and about $70M$ the differences are mainly due to the presence of the $(\ell = 2, m = 2, n = 1)$ mode, the exponentially decaying mode that can be seen in the inlay (a fit of this mode yields quasinormal frequencies in agreement with perturbation theory). At times $t \lesssim 25M$ the difference is due to the initial burst.

III. QUASINORMAL MODE FREQUENCIES AND EXCITATION AMPLITUDES FROM NUMERICAL SIMULATIONS

A. Overview

The time evolution of perturbations of a Kerr black hole can be split into three stages. After a first burst of radiation depending on the source of the excitation, the perturbation field Φ undergoes exponentially damped oscillations (ringdown phase). Finally, in the tail phase (caused by backscattering of radiation off the background gravitational potential) the field follows a power-law decay. In this paper we focus on the ringdown stage. We extract the different multipole components of the numerical solution by integrating the scalar field against different spherical harmonics over surfaces of constant observer radius r :

$$\Phi_{\ell m}(r, t) = \int Y_{\ell m}^*(\theta, \phi) \Phi d\Omega, \quad (11)$$

where a star denotes complex conjugation. We usually consider multipole components up to $\ell = 4$ and all values of m ($|m| \leq \ell$). By adding up the contributions of all multipoles one should recover the full scalar field:

$$\int_r \Phi^2 d\Omega = \sum_{\ell=0}^{\infty} \sum_{m=-\ell}^{\ell} (\Phi_{\ell m})^2. \quad (12)$$

As already mentioned, the rotation of the black hole and numerical errors can excite multipole components which are not present in the initial data. The above property can be used to check for the existence of overtones or modes with $\ell > 4$ that are not explicitly extracted but might be present in the solution (e.g. due to rotational mode mixing, numerical errors, or both). Multipoles with $m \neq 0$ require some care. The spherical harmonics $Y_{\ell m}(\theta, \phi)$ are given by

$$Y_{\ell m}(\theta, \phi) = \sqrt{\frac{2\ell + 1}{4\pi} \frac{(\ell - m)!}{(\ell + m)!}} P_{\ell}^m(\cos \theta) e^{im\phi}, \quad (13)$$

where $P_\ell^m(\theta)$ is a real function (an associated Legendre polynomial). Therefore the initial data of a pure multipole with $m \neq 0$ will be complex. Given that the evolution equations are linear, we can evolve the real and imaginary parts of Φ separately, and obtain the complex solutions for positive and negative m by linear combinations of the form

$$\Phi_{\ell m} = \mathcal{R}(\Phi_{\ell m}) + i\mathcal{I}(\Phi_{\ell m}), \quad (14a)$$

$$\Phi_{\ell -m} = \mathcal{R}(\Phi_{\ell m}) - i\mathcal{I}(\Phi_{\ell m}). \quad (14b)$$

This point is important for the extraction of the relative amplitude of corotating and counterrotating modes. In fact, as stressed (for example) in Ref. [8, 29], QNMs of Kerr black holes always come “in pairs”. In the Kerr case, for a given multipole (ℓ, m) we have to solve an eigenvalue problem to determine both the quasinormal frequencies $\omega_{\ell mn}$ and the angular separation constant $A_{\ell mn}$ (not to be confused with the mode amplitude $\mathcal{A}_{\ell mn}$ introduced below), used to separate the angular and radial dependence of the Teukolsky equation and write it as two ordinary differential equations. For *each* $(\ell, m \neq 0)$ and $j \neq 0$ the eigenvalue problem admits *two* sets of solutions. In addition to (ℓ, m) , we label the modes of each set by the overtone index n , denoting the frequencies by $\omega_{\ell mn}^{(i)}$ ($i = 1, 2$). For given (ℓ, m, n) , the solutions corresponding to the two different sets have different values of $\omega_{\ell mn}$ (and also of $A_{\ell mn}$):

$$\omega_{\ell mn}^{(1)} \neq \omega_{\ell mn}^{(2)}.$$

Both the real and imaginary parts are different. In fact, the real part of one of the frequencies is positive and the other one is negative:

$$\mathcal{R}(\omega_{\ell mn}^{(1)}) > 0, \quad \mathcal{R}(\omega_{\ell mn}^{(2)}) < 0.$$

If we consider instead the frequencies corresponding to the pair $(\ell, -m)$, they are related to those of (ℓ, m) by a simple symmetry property:

$$-\mathcal{R}(\omega_{\ell mn}^{(i)}) = \mathcal{R}(\omega_{\ell -mn}^{(j)}), \quad \mathcal{I}(\omega_{\ell mn}^{(i)}) = \mathcal{I}(\omega_{\ell -mn}^{(j)}), \quad (A_{\ell mn}^{(i)})^* = A_{\ell -mn}^{(j)}, \quad (i, j = 1, 2; i \neq j). \quad (15)$$

In this sense, any solution with positive m is nothing but the “mirror image” of a solution with opposite real part and opposite m (see Fig. 6 of [8] for an illustration of this). For $m = 0$ (or for any value of m in the Schwarzschild case) the two “mirror solutions” are degenerate in modulus of the frequency and damping time. However, in general, a multipolar component with a given (ℓ, m) will always contain a superposition of *at least* two different damped exponentials. Because of this, it is enough to consider only one frequency for each mode $[(\ell, m)$ or $(\ell, -m)]$, since the other two frequencies are obtained through this symmetry property; we follow the standard convention of considering, for each mode, the frequency with positive real part. Below we will discuss in detail the excitation of these modes, extending previous work by Krivan *et al.* [26].

When the perturbation field is in the quasinormal ringing regime, it can be expanded as a QNM sum of the form

$$\Phi_{\ell m}(r, t) \approx \mathcal{R} \left\{ \sum_{n=0}^{\infty} \mathcal{A}_{\ell mn} e^{i c_{\ell mn}} e^{-i \omega_{\ell mn} (t - t_0)} \right\}, \quad (16)$$

where $\mathcal{A}_{\ell mn}$ is the amplitude of the n -th overtone with angular structure given by the pair (ℓ, m) , $c_{\ell mn}$ its phase, $\omega_{\ell mn}$ its complex quasinormal frequency and t_0 (which to a first approximation we assume to be the same for all modes) marks the time at which the quasinormal regime starts.

The extraction of gravitational waves from numerical simulations of the full Einstein equations requires the observer to be located far away (in the wave zone). For the extraction of QNM frequencies, on the other hand, it is not problematic to place the observer close to the black hole, since an observer at any point in the space time is in general expected to measure the same frequencies. In fact, a small r is better suited for extracting quasinormal frequencies from our simulations simply because outer boundary effects pollute our waveform later, and the ringing regime can be observed for a longer time. The availability of a longer ringdown waveform improves the accuracy of the fitting procedure that we apply to extract the frequencies.

The effect of the observer’s location on the result is illustrated in Table I, where we list the frequencies of $(\ell = 2, m = \pm 2)$ fundamental modes for a Kerr black hole with spin $j = 0.9$ as measured by observers at radii $r = 5M$, $20M$ and $40M$. We picked $t_0 = r + r_0$ in Eq. (16) and $A = 0$, $B = 1$ in Eq. (10). The results presented in this Table are discussed in more detail below (Sec. III C). Here we simply remark that quasinormal frequencies measured at different radii are very close to the analytical predictions, supporting the statement that the observer does not need to be far away from the black hole to extract the correct ringdown frequencies. Indeed, *for these particular simulations* the relative error increases with r : the main reason, as explained, is that observers located at large radii see boundary effects earlier, so they can only measure a shorter ringdown waveform with respect to observers closer to the black hole.

Table I: Quasinormal frequencies computed by Leaver’s continued fraction method (here labeled “perturb.”) and by our time domain simulations, with the associated relative differences. We use 21×21 points in the angular direction on each block and a resolution of $M/10$ in the radial direction. For $j = 0.9$ we compare the frequencies as seen by observers located at different radii r . Observers at larger radii measure frequencies with larger errors, since boundary effects start to contaminate the waveform earlier.

r	j	l, m	$\omega_{\text{perturb.}}$	$\omega_{\text{numerical}}$	rel. difference (Re,Im)
$5M$	0.0	2, 0	$0.48364 - 0.09676i$	$0.48364 - 0.09676i$	$< 10^{-5}$
	0.5	2, 0	$0.49196 - 0.09463i$	$0.49190 - 0.09469i$	$4.27 \times 10^{-4}, 6.34 \times 10^{-4}$
	0.5	2, -2	$0.42275 - 0.09562i$	$0.42281 - 0.09569i$	$1.42 \times 10^{-4}, 7.32 \times 10^{-4}$
	0.5	2, 2	$0.58599 - 0.09349i$	$0.58589 - 0.09339i$	$1.71 \times 10^{-4}, 1.07 \times 10^{-3}$
	0.9	2, 0	$0.51478 - 0.08641i$	$0.51471 - 0.08646i$	$1.36 \times 10^{-4}, 5.79 \times 10^{-4}$
	0.9	2, -2	$0.38780 - 0.09379i$	$0.38781 - 0.09339i$	$2.58 \times 10^{-5}, 4.26 \times 10^{-3}$
	0.9	2, 2	$0.78164 - 0.06929i$	$0.78144 - 0.06955i$	$2.56 \times 10^{-4}, 3.75 \times 10^{-3}$
	0.98	2, 2	$0.89802 - 0.04090i$	$0.90940 - 0.04018i$	$1.27 \times 10^{-2}, 1.76 \times 10^{-2}$
	0.98	2, -2	$0.38177 - 0.09338i$	$0.38234 - 0.09743i$	$1.49 \times 10^{-3}, 4.34 \times 10^{-2}$
$20M$	0.9	2, -2	$0.38780 - 0.09379i$	$0.38694 - 0.09471i$	$2.22 \times 10^{-3}, 9.81 \times 10^{-3}$
	0.9	2, 2	$0.78164 - 0.06929i$	$0.78244 - 0.06670i$	$1.02 \times 10^{-3}, 3.74 \times 10^{-2}$
$40M$	0.9	2, -2	$0.38780 - 0.09379i$	$0.38406 - 0.09958i$	$9.64 \times 10^{-3}, 6.17 \times 10^{-2}$
	0.9	2, 2	$0.78164 - 0.06929i$	$0.78292 - 0.06618i$	$1.64 \times 10^{-3}, 4.49 \times 10^{-2}$

B. The time shift problem

Here we discuss the so-called *time-shift problem*, how it affects the extraction of quasinormal frequencies and amplitudes from numerical simulations, and a possible way to address it. Even though in this paper we consider scalar perturbations, the discussions of this and other sections apply also to other types of black hole perturbations.

The standard approach is to choose t_0 in Eq. (16) using some approximate calculation based, for example, on the location of the initial data and the time it would take for initial data to be scattered by the black hole potential and reach the observer, usually assuming that perturbations propagate with coordinate speed one (as they would in flat spacetime). Criteria like this are well motivated and provide a good guess, but there is still an uncertainty in t_0 . For example, the coordinate speed of the perturbation in a curved background in general will not be one. One might expect that such a small uncertainty would not influence the extraction of physically relevant quantities. However, as we discuss below, this is not the case: there are quantities of interest to gravitational wave detection which have a strong dependence on t_0 . Following the existing literature, we will call this the *time-shift problem*.

Suppose the starting time t_0 is subject to an uncertainty δ_0 . Under a change

$$t_0 \rightarrow t_0 + \delta_0, \quad (17)$$

the amplitude and phase of each mode change according to

$$\mathcal{A}_{\ell mn} \rightarrow \mathcal{A}'_{\ell mn} = \mathcal{A}_{\ell mn} e^{-\delta_0 \mathcal{I}(\omega_{\ell mn})}, \quad (18a)$$

$$c_{\ell mn} \rightarrow c'_{\ell mn} = c_{\ell mn} + \delta_0 \mathcal{R}(\omega_{\ell mn}). \quad (18b)$$

That is, an uncertainty in t_0 induces a linear uncertainty in the phase, and an *exponential* uncertainty in the amplitude. Fortunately other quantities are largely independent of this uncertainty: for example, the QNM frequencies $\omega_{\ell mn}$ are unaffected by δ_0 .

How large can we allow this exponential amplification of errors to be? Let us require the amplitude uncertainty induced by the starting-time uncertainty δ_0 to be less than some small number ϵ , that is

$$\left| \frac{\mathcal{A}'_{\ell mn} - \mathcal{A}_{\ell mn}}{\mathcal{A}_{\ell mn}} \right| = \left| e^{-\delta_0 \mathcal{I}(\omega_{\ell mn})} - 1 \right| < \epsilon.$$

For small ϵ this implies

$$|\delta_0| \lesssim \left| \frac{\epsilon}{\mathcal{I}(M\omega_{\ell mn})} \right| M. \quad (19)$$

For the $\ell = 2$ fundamental scalar mode in the Schwarzschild background (which is spherically symmetric, so that the choice of m becomes irrelevant) $|\mathcal{I}(M\omega_{200})| = 0.09676 \simeq 10^{-1}$. In other words, if we want to determine the amplitude of this mode within 1% ($\epsilon = 10^{-2}$) we need to know t_0 with an uncertainty $\delta_0 \lesssim 0.1M$. Constraints on δ_0 are even tighter for overtones, since they decay faster and the exponential propagation of errors is more dramatic.

In practice, what is most interesting is the *relative* amplitude between different modes. Under a change of the form (17) this relative amplitude changes according to

$$\frac{\mathcal{A}_{\ell mn}}{\mathcal{A}_{\ell' m' n'}} \rightarrow \left(\frac{\mathcal{A}_{\ell mn}}{\mathcal{A}_{\ell' m' n'}} \right)' = \frac{\mathcal{A}_{\ell mn}}{\mathcal{A}_{\ell' m' n'}} e^{-\delta_0 \mathcal{I}(\omega_{\ell mn} - \omega_{\ell' m' n'})}. \quad (20)$$

Following the same reasoning we find the constraint

$$|\delta_0| \lesssim \left| \frac{\epsilon}{M\mathcal{I}(\omega_{\ell mn} - \omega_{\ell' m' n'})} \right| M. \quad (21)$$

Consider for example the relative amplitude between the fundamental mode and the first overtone. For Schwarzschild black holes and small values of n the typical difference in the imaginary part of the frequency for two consecutive overtones ($\ell' = \ell$, $m' = m$, $n' = n + 1$) is

$$M\mathcal{I}(\omega_{\ell mn} - \omega_{\ell' m' n'}) \simeq 0.2.$$

Setting again $\epsilon = 10^{-2}$ the maximum allowed uncertainty on the starting time would be quite small: $\delta_0 \lesssim 0.05M$ (this presumably already precludes assuming that the perturbation propagates with speed one, as in flat spacetime).

Suppose we want to resolve corotating and counterrotating components of the fundamental mode with $\ell = 2$ (say, the components with $m = \pm\ell$). In the case of a spinning black hole background these QNM frequencies are different, but their imaginary parts are actually quite close for most values of the rotation rate [8, 29]. For example, looking at Table I we see that for spin $j = 0.5$ the difference is $|M\mathcal{I}(\omega_{220} - \omega_{2-20})| \simeq 0.00212$, so that $\delta_0 \lesssim 4.7M$. Even for a rapidly rotating black hole with $j = 0.9$ the difference is not as large as between a fundamental mode and its overtone: $M\mathcal{I}(\omega_{220} - \omega_{2-20}) \simeq 0.0245$, and $\delta_0 \lesssim 0.4M$.

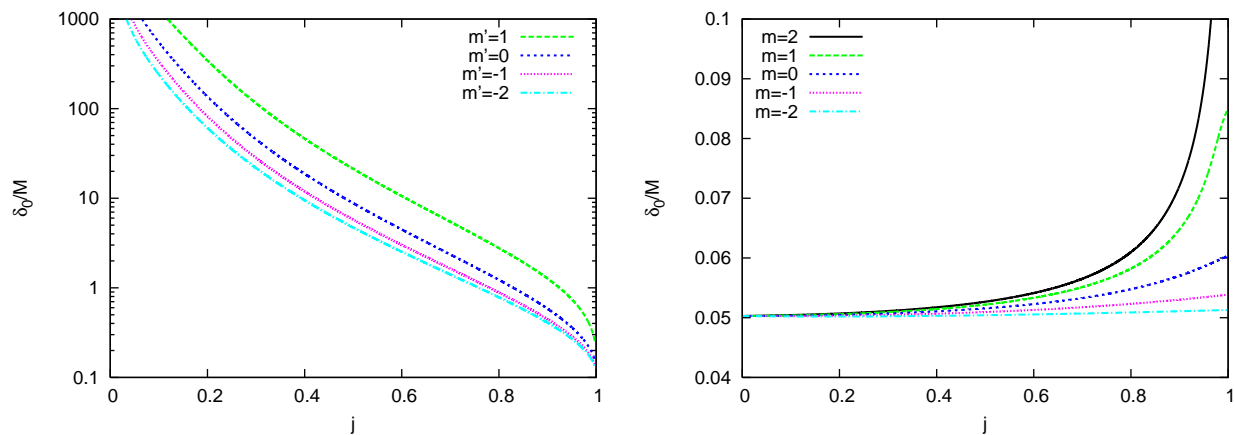


Figure 4: Critical uncertainty in the starting time, as defined by Eq. (21), assuming $\epsilon = 10^{-2}$. In the left panel we give the critical δ_0 for fundamental modes ($n = n' = 0$) with different angular dependence. For the first mode we assume $\ell = m = 2$; the second mode has $\ell' = 2$ and different values of $m' = 1, 0, -1, -2$ (lines from top to bottom). In the right panel we show the critical uncertainty in the relative amplitude of the fundamental mode and first overtone, i.e., $n = 0$ and $n' = 1$. Here we set $\ell = \ell' = 2$, consider all values of $m = m'$ and once again we assume $\epsilon = 10^{-2}$.

Critical starting-time uncertainties for $\epsilon = 10^{-2}$, general values of the spin and different pairs of modes are plotted in Fig. 4. Determining the relative amplitude of a fundamental mode and of the first overtone is generally harder, unless we consider corotating modes and near-extremal black holes, as we do in Sec. III F. The spin dependence of δ_0 is quite weak for overtones, but δ_0 can change by orders of magnitude for modes with different angular dependence ($\ell \neq \ell'$ or $m \neq m'$). For $j \lesssim 0.5$ the *time-shift problem*, as we defined it here, becomes irrelevant when we want to determine the relative amplitude of components with the same l and different m 's. The reason is simply that modes with different m 's have the same QNM frequency in the Schwarzschild limit, so that $\delta_0 \rightarrow \infty$. As a rule of

thumb, determining the relative amplitude of angular components with the same l and different m 's is harder for large rotation. However, as we said before, even for $j = 0.9$ the critical uncertainty is $\delta_0 \gtrsim 0.4M$, an order of magnitude larger than the typical uncertainty to resolve overtones (which in most cases is $\sim 0.05M$). Most of the qualitative features of Fig. 4 are also seen in the experimental problem of resolving different QNMs in the actual detection of a ringdown signal (compare e.g. Figs. 3, 4 and 18 of [8]).

In Sec. III E and Sec. III F we will study in more detail the extraction of corotating and counterrotating modes and of overtones, respectively. In preparation for this study, in the next Section we outline the general method by which we extract quasinormal frequencies from our numerical waveforms.

C. Extraction of QNM frequencies by an optimal choice of the fitting interval

Once we have the different multipole components of the numerical solution, we analyze them by applying a fitting procedure to each of these components. Since each mode decays exponentially while oscillating with its quasinormal frequency, the obvious function to fit the numerical waveform is Eq. (16), where the free parameters are the amplitudes, phases and frequencies. As discussed in Sec. III F, only in some cases we have been able to fit for overtones, in the sense of getting their expected quasinormal frequencies with reasonable accuracy. However, as described below, the residual that we get by truncating the sum at the fundamental mode is already quite small (see also Fig. 3).

In this subsection we are interested in extracting the quasinormal frequencies from our numerical data. To a very good approximation the frequencies are independent of t_0 , and we can therefore pick any value for the latter. We still need to find a good choice for the time interval $[T_i, T_f]$ over which the ringdown dominates and the fitting procedure works best. Since in principle the parameters obtained from the fitting might depend on the choice of this time interval, we discuss our procedure in detail.

Only during the ringdown phase does the waveform have the functional behavior of Eq. (16), so the time interval $[T_i, T_f]$ should not include the transient regime and the tail phase. For our simulations we found it reasonable to pick $T_f = 150M$, since for $T > T_f$ the system typically goes into the tail phase. The choice of T_i is more delicate: small values would bring the fitting time window out of the ringdown phase, but large values would make the fitting interval small and the resulting fit inaccurate. We decided to take a pragmatic approach: for different values of T_i we compute the (relative) residual $R(T_i, t_0)$ between the fitted function and the numerical data, which we define as

$$R(T_i, t_0) = \left(\sum_{t_j=T_i}^{T_f} |\Phi_{\text{data}}(t_j) - \Phi_{\text{fit}}(t_j, t_0)| \right) \left(\sum_{t_j=T_i}^{T_f} |\Phi_{\text{data}}(t_j)| \right)^{-1} \quad (22)$$

We then choose the value of T_i that minimizes the residual. In a very well defined sense, this gives an optimal choice for T_i . In principle one could use other norms (for example, a sum over squares instead of a sum over absolute values), but we checked that this does not affect significantly the results of this paper. Choosing the value of T_i that minimizes the residual defined above should not be confused with the minimization procedure done at each T_i to get the fit itself.

Instead of extracting the quasinormal frequencies through a fitting procedure, in principle one could also perform a Fourier transform of the solution, as in Ref. [26]. However we have found that the fitting procedure provides us with far superior accuracy, even in cases with relatively few sampling points. Nonetheless we compared to the results that we obtained by Fourier analysis and found consistency between both methods.

Figure 5 shows the residual as a function of T_i for one of our simulations (the one corresponding to spin $j = 0.5$ and $\ell = m = 2$ initial data in Table I). The residual is independent of the choice of excitation time t_0 , since a change in t_0 is just absorbed in the amplitude of the fitting function, leaving the other fitting quantities unaffected.

Since the black hole's spin is non zero, both $m = 2$ and $m = -2$ modes are present in the solution. Here we discuss only the $m = 2$ part of the numerical solution. The $m = -2$ part behaves similarly (in Sec. III E we present a detailed study of the relative amplitudes of corotating and counterrotating modes).

From Fig. 5 we see that $R(T_i, t_0)$ has a rather sharp local (and global) minimum. By computing the derivative (through finite differences) of the residual with respect to T_i we find that the minimum is located at $T_i = (59.65 \pm 0.025)M$. The uncertainty refers to the difference between two consecutive values of T_i , which is in turn given by the time step for this simulation: $\Delta t = 0.025M$.

Figure 6 shows the real and imaginary parts of the frequency extracted from the same simulation as a function of T_i . By evaluating them at $T_i = (59.65 \pm 0.025)M$ we get $\omega_R = 0.585887 \pm 1 \times 10^{-6}$ and $\omega_I = 0.0933851 \pm 5 \times 10^{-7}$.

Figure 6 also reveals that ω changes very little within the interval $50M \lesssim T_i \lesssim 80M$. Since our choice of T_i is by no means unique—for example a different definition of the residual would slightly shift T_i —this plateau in the frequencies guarantees that the physical quantities we extract are not too sensitive to that uncertainty. This means that the errors in our numerically extracted QNM frequencies due to the choice of T_i are quite small.

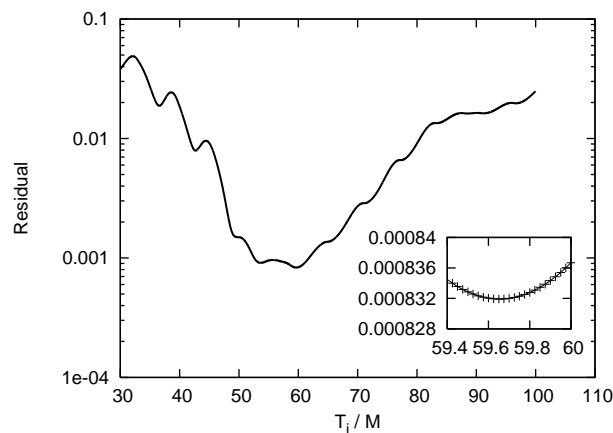


Figure 5: Residual in the fit, as defined in Eq. (22), as a function of the initial time for the fitting T_i . Looking at the minimum of the residual we can determine T_i with high precision. This plot corresponds to a simulation with spin $j = 0.5$, $\ell = m = 2$ initial data with $A = 0$, $B = 1$ and a radial resolution $\Delta r = M/10$.

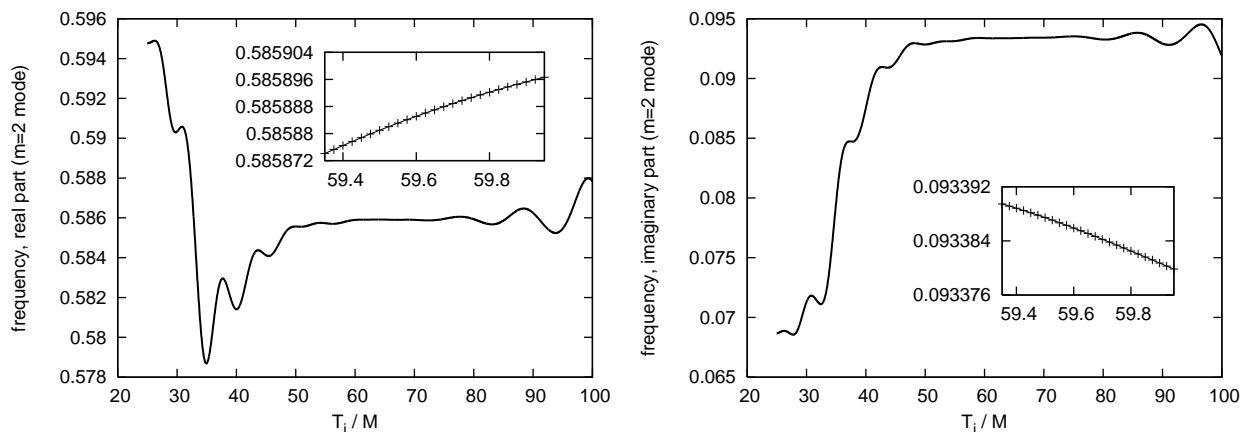


Figure 6: The left and right panels show the real and imaginary parts of the quasinormal frequencies extracted from the simulations in Fig. 5. From the optimal starting time determined by minimizing the residual, $T_i = (59.65 \pm 0.025)M$ (see previous figure), we find $\omega_R = 0.585887 \pm 1 \times 10^{-6}$ and $\omega_I = 0.0933851 \pm 5 \times 10^{-7}$.

We are now ready to examine the quasinormal frequencies obtained from our numerical data in the way just described. Table I shows the frequencies computed in [16] using Leaver’s continued fraction method for perturbed Kerr black holes with spin $j = 0, 0.5$, and 0.9 (here labeled *perturb.*). Along with these frequencies we list values extracted from our time domain evolutions (labeled *numerical*) and the relative differences between the two. The numerical values were obtained by evolving different initial data sets with $A = 0$ and $(\ell = 2, m = 0, \pm 2)$ in Eq. (10), and fitting for the multipoles present in the initial data (we discuss the additional multipoles generated by rotational mode mixing below). For $j = 0$ the frequencies do not depend on m , therefore we only show results for $m = 0$. Even with a relatively modest resolution, the differences on quasinormal frequencies from our three-dimensional simulations in Table I are between one and two orders of magnitude smaller than the ones reported in previous two-dimensional, axisymmetric simulations of gravitational perturbations [26].

D. Rotational mode mixing

In Sec. IID we described our initial data family sets, which were expanded in spherical harmonics. Since the Kerr background is not spherically symmetric we should not expand the perturbation in terms of spherical harmonics, but (more rigorously) in terms of the spin-weighted spheroidal harmonics ${}_s S_{\ell m}(a\omega)$, where s is the spin weight of

the perturbing field, $a = jM$ is the black hole spin parameter, and ω is the frequency in a Fourier expansion of the perturbation (a quantitative discussion of spin-weighted spheroidal harmonics and more references can be found in [30]). However, as first shown by Press and Teukolsky [31], the ${}_s S_{\ell m}$'s may be expanded as a power series in $a\omega$:

$${}_s S_{\ell m} = {}_s Y_{\ell m} + (a\omega) \sum_{\ell' \neq \ell} c_{\ell' \ell m} {}_s Y_{\ell' m} + O(a\omega)^2. \quad (23)$$

Here ${}_s Y_{\ell m}$ denotes a spin-weighted spherical harmonic of spin-weight s . In this paper we focus on scalar perturbations ($s = 0$), in which case the spin-weighted spherical harmonics reduce to ordinary spherical harmonics. The coefficients $c_{\ell' \ell m}$ are related to the more familiar Clebsch-Gordan coefficients [30, 31]. As a result of (23), and because of the orthogonality of the (spin-weighted) spherical harmonics, inner products of different spheroidal harmonics will be given by inner products of *spherical* harmonics with higher-order corrections in $a\omega$. At least for small $a\omega$, we may expect these contributions to be small. In fact, the corrections turn out to be small even for moderately large values of $a\omega$ (see [30] for an explicit calculation of the inner products at the QNM frequencies). Nevertheless, using spherical harmonics instead of spheroidal harmonics can induce a small amount of mode-mixing in the initial data.

For a spherically symmetric background spacetime, initial data with different values of ℓ evolve separately and the angular structure of each mode is preserved during evolution. On the other hand, for a Kerr background with nonzero spin, modes with different values of ℓ do couple and furthermore, modes that are not present in the initial data can be excited during evolution. This may make it necessary to increase the angular resolution compared to the non-rotating case to resolve the higher ℓ modes generated during evolution. However, the decay rate of these modes increases with ℓ , so even when modes with higher values of ℓ are generated during evolution, they do not dominate. Therefore, we found that if we accurately resolve the angular structure initially, the same is in general true for the whole evolution.

Figure 7 illustrates rotational mode coupling for non-zero spin backgrounds (see also [32] and [33] for numerical studies of mode-mode coupling). Since modes with same m but different ℓ can couple to each other, we show the extracted ($\ell = 4, m = 2, n = 0$) waveform (for three simulations with different spin parameters) excited by initial data whose angular dependence is given by an $\ell = m = 2$ spherical harmonic. As expected, the rotationally-induced excitation of the ($\ell = 4, m = 2$) mode typically increases with spin. Some additional mode mixing is an artifact of the symmetry of our computational grid. This ‘‘spurious’’ mode mixing is present also for $j = 0$, but it converges to zero as we increase the angular resolution. All other modes we extract, up to $\ell = 4$ and all allowed values of m , are within roundoff error throughout the simulations.

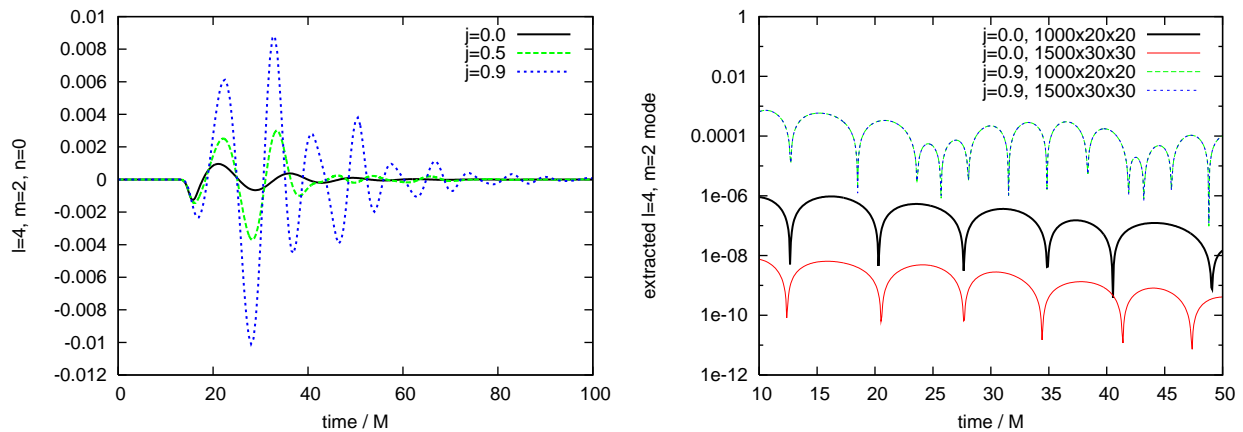


Figure 7: The left panel shows the extracted ($\ell = 4, m = 2, n = 0$) waveform for three simulations with different spin parameters as seen by an observer at $r = 5M$. The initial data are a pure ($\ell = m = 2$) mode and are set up according to Eq. (10) with $A = 0$, $B = 1$ and $r_0 = 20M$. For zero spin the different multipole components of the solution should evolve independently and no modes besides the one in the initial data should be excited, while for non-zero spin modes with different ℓ but same m do couple [26]. In the Schwarzschild case the ($\ell = 4, m = 2, n = 0$) waveform differs from zero due to our grid structure and discretization errors, but it converges to zero with increasing resolution. This is illustrated by the right panel, which shows the extracted ($\ell = 4, m = 2, n = 0$) amplitude for $j = 0$ and $j = 0.9$ from runs with two resolutions ($20 \times 20 \times 1000$ and $30 \times 30 \times 1500$ points per patch and outer boundaries at $100M$). Only for $j = 0.0$ the mode converges to zero.

Since we only extract QNMs up to $\ell = 4$ we need to test whether there is a relevant contribution from higher modes that we do not extract explicitly. In the absence of $\ell > 4$ modes, summing up all extracted modes up to $\ell = 4$ we

should recover the full field, according to Eq. (12). The result of this test for a spinning black hole with $j = 0.9$ is shown in Fig. 8: at the level of accuracy needed in the present work, extracting modes with $\ell \leq 4$ is sufficient.

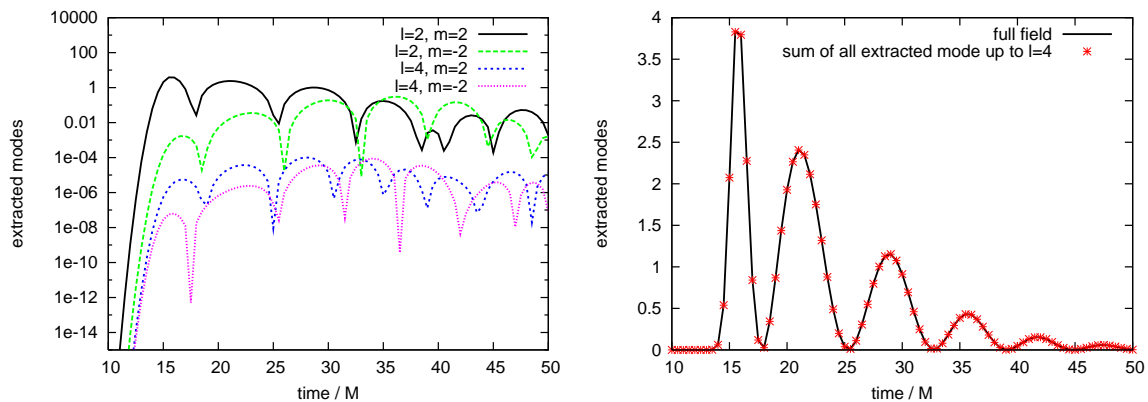


Figure 8: Results from a run with initial data parameters $\ell = m = 2$ and spin $j = 0.9$. The left panel shows the square of the amplitude of all modes up to $\ell = 4$ which are not within the roundoff error. The right panel shows the sum over the square of those modes compared to the integral over a sphere of the full field squared: As expressed in equation 12 the two curves lie on top of each other, and there is no relevant contribution from higher modes.

E. Relative amplitude of corotating and counterrotating modes

We know that when the solution is in the quasinormal ringing regime, it will behave according to Eq. (16). In the previous subsection we have verified through our simulations the values predicted in Ref. [16] for the frequencies. We now also want to verify the amplitudes of each mode, as predicted in that same reference.

Assume that the observer and the initial data are located far away from the black hole (these assumptions underlie the “asymptotic approximation” adopted in [16, 34]). From Eq. (4.15) of [16], when $B = 0$ the response of the black hole in the ringdown phase should be well approximated by a QNM decomposition of the form

$$\Phi_{\ell m}(r, t) \approx -\frac{r_0}{r} \sqrt{\pi} \sigma \mathcal{R} \left\{ \sum_{n=0}^{\infty} (iA\omega_{\ell mn}) B_{\ell mn} e^{-\sigma^2 \omega_{\ell mn}^2 / 4} e^{-i\omega_{\ell mn}(t-r_0-r_*)} \right\}, \quad (24)$$

In our simulations we set $A = 0$, in which case it can easily be shown that the previous expression becomes

$$\Phi_{\ell m}(r, t) \approx -\frac{r_0}{r} \sqrt{\pi} \sigma B \mathcal{R} \left\{ \sum_{n=0}^{\infty} B_{\ell mn} e^{-\sigma^2 \omega_{\ell mn}^2 / 4} e^{-i\omega_{\ell mn}(t-r_0-r_*)} \right\}, \quad (25)$$

With respect to [16] we added an extra factor r_0/r . This is because Eq. (4.15) in [16] refers to the Sasaki-Nakamura function $X_{\ell m}^{(0)}(r, t)$, which is related to the Teukolsky function $\Phi_{\ell m}(r, t)$ that we are using in our evolutions by the relation $X_{\ell m}^{(0)}(r, t) = (r^2 + a^2)^{1/2} \Phi_{\ell m}(r, t)$ (see the discussion in Appendix C of [16]). We are interested in large values of r , for which the asymptotic approximation holds and $X_{\ell m}^{(0)}(r, t) \simeq r \Phi_{\ell m}(r, t)$. The transformation between the Teukolsky and Sasaki-Nakamura functions must also be taken into account when comparing the initial data in Eq. (4.14) of [16] with our initial data, Eq. (10). Assuming $\sigma \ll r_0$ and $r \gg 1$ this comparison yields the normalization factor r_0 in the equations above.

The scalar QNM frequencies $\omega_{\ell mn}$ and the scalar excitation factors $B_{\ell mn}$ are listed in Table I and Table III of [16], respectively. In that reference and in Eq. (24) Boyer-Lindquist coordinates are used; since in our simulations we use Kerr-Schild coordinates we need to transform Eq. (24) appropriately. Since Φ is a scalar, the transformation is straightforward. The transformation of the initial data is more subtle, since the slices are different. One would expect that whenever the asymptotic approximation is valid the difference between the slices should not be too important. The results discussed below and explicit comparisons between evolutions using both coordinate systems in the non-spinning case [35] confirm this expectation. Details on how we transform the initial data and the field itself are given in Appendix A.

To check the accuracy of Eq. (25), in the rest of this section we analyze evolutions of different initial data sets, all of them consisting of a combination of $(\ell = 2, m = 2)$ and $(\ell = 2, m = -2)$ modes with $A = 0$ and $B = 1$. We numerically explore the dependence of the amplitudes of the counter- and co-rotating *fundamental* modes (in the next subsection we will study overtones) on the width σ of the initial data [cf. Eq. (10)]. In order to assess more quantitatively the effect of the *time-shift problem* (see Sec. III B) we first compare the value of the width maximizing these amplitudes. Given that all the initial data sets that we consider are centered at the same radius, we can make the reasonable assumption that locally (that is, around the width for which the amplitudes are maximal) t_0 is approximately the same for each set. If t_0 were *exactly* the same, the value of t_0 used would not change the width at which the maximum amplitude is located, since changes in t_0 would only involve a global rescaling of all amplitudes, as discussed in Sec. III B. Therefore the hope is that within the setting described for our simulations the width for which the amplitudes are maximal does not depend too sensitively on t_0 .

The numerical results shown here were obtained with the same number of points in the angular direction as above. We used half the resolution in the radial direction (that is, $\Delta r = M/5$) for a rough scan of a large σ range, and again the original resolution around the maxima of the amplitudes. We chose initial data with varying widths σ , $r_0 = 20M$ (as in the simulations above) and an observer at $r = 40M$, for which the asymptotic approximation holds reasonably well [35]. We picked $t_0 = r_{\text{initial data}} + r$ (that is, $t_0 = 60M$ in the cases considered), which is approximately the time the initial data pulse needs to propagate to the black hole and back to the observer.

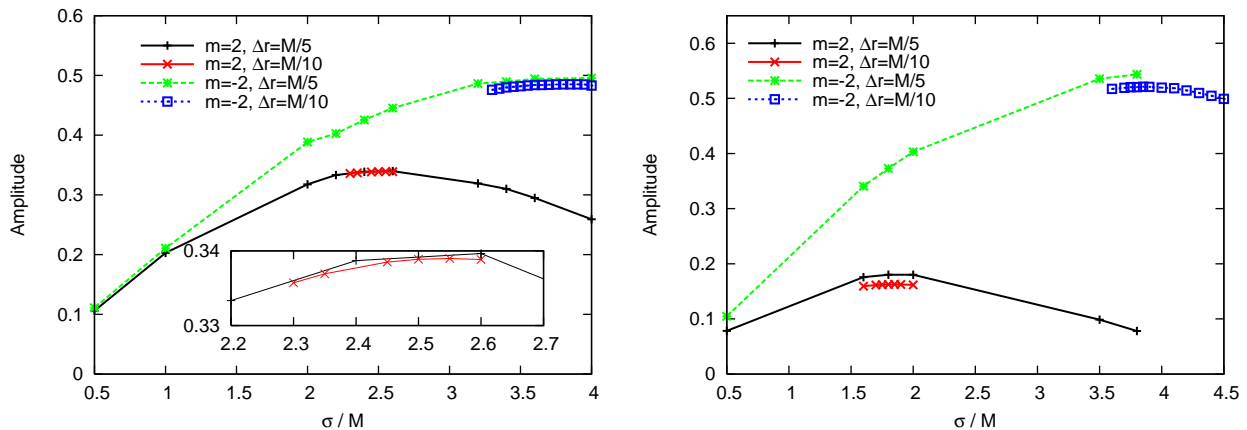


Figure 9: Numerically obtained excitation amplitudes of the $\ell = |m| = 2$ fundamental modes assuming an observer location $r_{\text{obs}} = 40M$ and a ringdown starting time $t_0 = 60M$. The left panel refers to a black hole with spin $j = 0.5$. According to predictions from perturbation theory in the asymptotic approximation [cf. Eq. (24) and the following discussion] the maximum for $m = 2$ should be located at $\sigma_{220} = 2.445$, while the value that we obtain from our simulations is $\sigma_{220} = 2.55 \pm 0.05$ (the uncertainty describing the difference between consecutive values of σ used in our simulations: $\Delta\sigma = 0.05$). Similarly, for $m = -2$ the width at the maximum should be $\sigma_{2-20} = 3.434$, while we obtain $\sigma_{2-20} = 3.875 \pm 0.075$. The right panel, in turn, refers to a black hole with spin $j = 0.9$. In this case the theoretical (numerical) maxima are located at $\sigma_{220} = 1.816$ ($\sigma_{220} = 1.85 \pm 0.05$) and $\sigma_{2-20} = 3.758$ ($\sigma_{2-20} = 3.85 \pm 0.05$), respectively. The inset in the left panel is a zoom around the maximum for $j = 0.5$ and $m = 2$. As discussed in the text, an uncertainty in the excitation time of $0.09M$ would already explain the difference between the predicted location of the maxima and our numerical results.

Figure 9 and (more quantitatively) Tables II and III show the excitation amplitudes as functions of the width of the Gaussian σ from our numerical simulations. At first our results could be interpreted as an approximate verification of the predictions of [16]. However, if one takes into account the limitations imposed by the *time-shift problem*, the agreement can in fact be considered excellent. For example, take the $j = 0.5, m = -2$ case, which is the one where the difference between the theoretical and numerical values is largest. The theoretical maximum is located at $\sigma = 3.434M$, while the numerical value is $\sigma = (3.875 \pm 0.075)M$ (the uncertainty indicating the difference between consecutive values of σ). The relative numerical amplitude between $\sigma = 3.45M$ and $\sigma = 3.85M - 3.9M$ from our simulations is ≈ 1.008 (see Table II). If the values of t_0 for these two widths differ by $\approx 0.09M$, the amplitude corresponding to $\sigma = 3.45M$ would actually be larger than the one of $\sigma = 3.85M - 3.9M$ and would therefore shift the maximum to the predicted value of $3.45M$. Recalling that we used $t_0 = 60M$, a very modest uncertainty in the *relative* ringdown starting time ($\approx 0.4\%$) would shift the maximum to the theoretical value. We also assumed the same excitation time t_0 for all the initial data sets when fitting our numerical data. Whenever such assumption is a good approximation, the precise value of t_0 should not affect the location of the width for which the excitation amplitudes is maximal. In particular, the approximation should be good if the initial data pulses are relatively narrow. However,

Table II: Excitation amplitudes for $j = 0.5$, $\ell = 2$ and $n = 0$ for initial perturbations of variable Gaussian width σ , as displayed in Fig. 9. The observer location in these runs is $r = 40M$. Highlighted are the maxima in the amplitudes of the different m -modes. Also shown are the relative amplitudes of the two modes, and the relative differences between the values predicted by perturbation theory and the ones extracted from our numerical simulations. The amplitudes are given for the wave expressed in Boyer Lindquist coordinates (see appendix A for details) and are multiplied by a factor of r/r_0 to get them in an observer independent form.

σ	numerical results			perturbation theory			relative difference
	\mathcal{A}_{220}	\mathcal{A}_{2-20}	$\mathcal{A}_{2-20}/\mathcal{A}_{220}$	\mathcal{A}_{220}	\mathcal{A}_{2-20}	$\mathcal{A}_{2-20}/\mathcal{A}_{220}$	$\mathcal{A}_{2-20}/\mathcal{A}_{220}$
2.30	0.3357	0.411	1.22	0.315	0.419	1.33	0.080
2.35	0.3369	0.410	1.22	0.314	0.423	1.35	0.097
2.45	0.3385	0.420	1.24	0.311	0.430	1.38	0.103
2.50	0.3389	0.425	1.25	0.310	0.433	1.40	0.102
2.55	0.3390	0.430	1.27	0.308	0.436	1.42	0.104
2.60	0.3388	0.435	1.28	0.306	0.439	1.43	0.105
3.30	0.315	0.476	1.51	0.253	0.449	1.77	0.149
3.35	0.311	0.478	1.54	0.248	0.448	1.81	0.149
3.40	0.308	0.480	1.56	0.243	0.446	1.84	0.151
3.45	0.304	0.481	1.58	0.238	0.445	1.87	0.154
3.50	0.301	0.482	1.60	0.233	0.443	1.90	0.158
3.55	0.297	0.483	1.63	0.228	0.441	1.93	0.159
3.60	0.293	0.484	1.65	0.223	0.439	1.97	0.161
3.65	0.289	0.484	1.67	0.217	0.437	2.01	0.168
3.70	0.285	0.4843	1.70	0.212	0.434	2.05	0.170
3.75	0.281	0.4848	1.73	0.207	0.432	2.09	0.173
3.80	0.276	0.4850	1.76	0.202	0.429	2.12	0.173
3.85	0.272	0.4851	1.78	0.196	0.425	2.17	0.178
3.90	0.267	0.4851	1.82	0.191	0.423	2.21	0.180
3.95	0.263	0.4849	1.84	0.186	0.419	2.25	0.182
4.00	0.259	0.4831	1.87	0.180	0.416	2.31	0.193

as σ increases, the possibility of the excitation time t_0 shifting around has to be taken into account, because the interaction time of the pulse with the black hole becomes longer and the interaction sets in well before the center of the pulse reaches the black hole. Taking all this into account, the agreement between numerical and perturbative results for the location of the maxima can be considered excellent. The situation for the amplitudes themselves is different, as discussed next.

Tables II and III show the predicted and extracted absolute and relative amplitudes for the co- and counterrotating modes $\mathcal{A}_{m=2}$, $\mathcal{A}_{m=-2}$. As expected, the prediction from perturbation theory works better for sharp pulses. The differences between the predicted and absolute values are of order a few percent for sharp pulses and grow with σ . For $\sigma = 4$ the difference is as large as $\sim 20\%$ and $\sim 60\%$ for $j = 0.5$ and $j = 0.9$, respectively (the actual amplitudes being larger than the predicted ones). These large differences in the relative amplitudes are mostly due to the amplitude of the corotating mode, the predicted and extracted amplitudes for the counterrotating one agree quite well. The fact that the location of the maxima, as discussed above, agrees very well despite the large differences in the amplitudes for larger σ can be easily explained: the location of the maxima for the corotating mode takes place at $\sigma \approx 1.85M$, which corresponds to a pulse which is sharp enough for perturbation theory to give a good prediction, while the maximum for the counterrotating mode is at a larger value of σ but, as we have discussed, the agreement between predicted and measured amplitudes is quite good for that mode.

Could this large difference in amplitudes be explained by the *time-shift problem*, as discussed in Sec. III B? Using Eq. (20) and assuming that t_0 is roughly the same for both modes we find that an uncertainty in the excitation time as large as $\delta_0 = \pm 5M$ would imply an uncertainty on the relative amplitudes of about $\pm 1.1\%$ for $j = 0.5$, and $\pm 13\%$ for $j = 0.9$. Therefore the uncertainty δ_0 does not seem to account for the differences that we find with respect to the predicted amplitudes. One possibility is that the excitation time t_0 is different for the two modes in a pair; but, if so, it is not clear then why our naive choice of t_0 is very good for the counterrotating mode and quite bad for the

Table III: Same as Table II for $j = 0.9$.

σ	numerical results			perturbation theory			relative difference
	\mathcal{A}_{220}	\mathcal{A}_{2-20}	$\mathcal{A}_{2-20}/\mathcal{A}_{220}$	\mathcal{A}_{220}	\mathcal{A}_{2-20}	$\mathcal{A}_{2-20}/\mathcal{A}_{220}$	$\mathcal{A}_{2-20}/\mathcal{A}_{220}$
1.60	0.1594	0.3156	1.98	0.1768	0.3683	2.08	0.05
1.70	0.1615	0.3319	2.06	0.1766	0.3857	2.18	0.06
1.75	0.1621	0.3399	2.10	0.1755	0.3990	2.27	0.08
1.80	0.1625	0.3476	2.14	0.1752	0.4022	2.30	0.07
1.85	0.1626	0.3553	2.18	0.1740	0.4101	2.36	0.07
1.90	0.1625	0.3629	2.23	0.1725	0.4177	2.42	0.08
2.00	0.1617	0.3775	2.33	0.1725	0.4323	2.51	0.07
3.60	0.0800	0.5173	6.47	0.0566	0.5259	9.30	0.30
3.70	0.0743	0.5192	6.99	0.0507	0.5235	10.32	0.32
3.75	0.0714	0.5204	7.29	0.0479	0.5220	10.89	0.33
3.80	0.0688	0.5204	7.56	0.0452	0.5203	11.51	0.34
3.85	0.0661	0.5212	7.89	0.0427	0.5184	12.15	0.35
3.90	0.0636	0.5208	8.19	0.0402	0.5162	12.85	0.36
4.00	0.0590	0.5194	8.81	0.0355	0.5114	14.41	0.39
4.10	0.0590	0.5184	8.79	0.0312	0.5059	16.20	0.46
4.20	0.0505	0.5144	10.19	0.0274	0.4997	18.25	0.44
4.30	0.0469	0.5098	10.88	0.0239	0.4929	20.64	0.47
4.40	0.0433	0.5047	11.65	0.0207	0.4854	23.41	0.50
4.50	0.0433	0.4991	11.52	0.0179	0.4774	26.63	0.57

corotating one. It is actually not clear why such a large disagreement happens only for the corotating mode, and not for the counterrotating one. The possibilities that the initial data and/or the observer are not far enough away for the asymptotic approximation to be valid, or that the disagreement is due to a lack of resolution, seem to be ruled out by one-dimensional studies in the non-spinning case [35]. Summarizing, even though the exact mechanism is not clear, all this suggests that the predicted amplitudes for the corotating mode in the asymptotic approximation are simply valid only for very sharp pulses, as the black hole spin increases.

To conclude, we want to discuss one aspect of our simulations, as shown in Figure 9. We see a rather large discrepancy between the amplitudes resulting from runs with resolution $\Delta r = M/5$ and $\Delta r = M/10$, especially for $j = 0.9$. That is a direct effect of decreasing accuracy in $\mathcal{I}(\omega_{\ell mn})$ when going to high spins (see Sec. III C) and the need for more resolution in those cases. The *location* of the maximum, however, is always consistent (that is, within the differences in σ used in the different initial data sets) between runs of different resolution. That is not surprising since the measured $\omega_{\ell mn}$ at a fixed resolution is roughly the same for all values of σ , and the value of σ that maximizes $\mathcal{A}_{\ell mn}$ only depends on the value of $\omega_{\ell mn}$.

F. Overtones and rapidly spinning black holes

As discussed in the introduction, a single complex quasinormal frequency contains enough information to determine the two parameters of a Kerr black hole (namely, its mass M and spin j). If one is able to detect a second mode from the same source, one can use this extra information for a consistency check that would increase the confidence in the interpretation of the measured data as signals from a perturbed black hole. An important question that might be answered by numerical relativity is whether more than one mode will be detectable by Earth- and space-based gravitational wave detectors. In Sec. III E we considered the relative amplitude of corotating and counterrotating modes; here we use our simulations to determine the relative excitation of overtones with the same angular dependence and $m > 0$. According to perturbation theory, in this case the damping time of the first overtone becomes comparable to the damping time of the fundamental mode for large spins (see Fig. 4). In addition, the excitation factor of higher overtones is usually larger than the excitation factor of the fundamental mode for large j [16]. This means that higher overtones are more likely to be detectable for fast spinning black holes. A detailed study of this topic is beyond the scope of this paper, but here we briefly discuss how we can extract information about overtones from our data and

determine which modes contribute most significantly to the waveform.

We perform simulations for different spins ($j = 0, 0.5, 0.9$, and 0.98). The initial data and numerical procedure are the same as in Sec. IID and IIE, with one exception: for spins $j \geq 0.9$ we found it necessary to increase the angular resolution. The simulations presented in this section used a resolution of 31×31 grid points on each block in the angular directions. This is not surprising, since for fast rotation we expect more dynamics in the angular directions.

The extraction of modes is done in principle according to Sec. III C. Extracting information about all modes present in the data can turn into a subtle problem, especially when the contributions of some modes is weak. One option is to first fit for the strongest mode present in the data, subtract the fit, fit for the next dominant mode and so on, repeating the procedure as long as an oscillatory exponential decay is seen in the data. However, when there are several modes with similar contributions we can just fit for all of them at the same time. This is exactly what we did for fundamental modes with different m in the previous subsection. When a single mode dominates the waveform the first strategy not only seems to be more meaningful, but also turns out to work better in practice. The results of this section were computed by a hybrid of these two methods, depending on the contribution of each mode (something that one can find out by, for example, looking at the dominant frequencies of the signal to fit).

Table IV shows the quasinormal frequencies of the overtones that we get from our simulations, using ($A = 0, B = 1$), $\sigma = M, r_0 = 20M$ and an observer at $r = 60M$. We find that the overtones for the $m = -2$ mode do not contribute enough to the waveforms to extract them from our data with decent accuracy, especially for high spins. The reason for this is that the imaginary part of their frequency is generally smaller than the one for the corresponding $m = 2$ mode, which makes them decay faster. The decay of the $m = 2$ mode, on the other hand, slows down considerably when increasing the spin. We numerically find that the excitation amplitude (at fixed t_0) increases with increasing spin. Those two effects combined make the extraction of overtones easier and more accurate in the high spin cases. Quite remarkably, for runs with spin $j = 0.9$ and above we can extract the quasinormal frequency for $n = 2$ with reasonable accuracy (see Table IV).

Table V compares the amplitudes of the three most dominant $l = 2$ modes, ($m = 2, n = 0$), ($m = -2, n = 0$) and ($m = 2, n = 1$), with the predicted asymptotic amplitudes of Eq. (24). Except for the $j = 0.98$ case, the difference between the predicted and extracted values for the relative amplitudes between a given mode and the fundamental $l = 2 = m$ one is of the order of a few percent for the fundamental mode and one order of magnitude larger for the first overtone.

Table IV: Comparison of quasinormal frequencies for the first overtones ($n = 1, 2$) of an $l = 2, m = 2$ mode, for black holes with varying spin, as predicted by perturbation theory and as extracted from our numerical simulations, along with their relative differences. This table is complementary to Table I, where we show the frequencies associated to the fundamental modes. The extraction of overtones becomes easier for rapidly rotating black holes, as explained in the text, allowing us to extract the frequencies of two overtones for high spins.

j	n	ω_{perturb}	$\omega_{\text{numerical}}$	rel. difference (Re, Im)
0.0	1	$0.46385 - 0.29560i$	$0.45651 - 0.28859i$	$1.58 \times 10^{-2}, 2.37 \times 10^{-2}$
0.5	1	$0.57344 - 0.28334i$	$0.54718 - 0.31722i$	$4.58 \times 10^{-2}, 1.20 \times 10^{-1}$
0.9	1	$0.77768 - 0.20801i$	$0.73737 - 0.19558i$	$5.18 \times 10^{-2}, 5.98 \times 10^{-2}$
0.9	2	$0.77043 - 0.34720i$	$0.52473 - 0.35319i$	$3.19 \times 10^{-1}, 1.73 \times 10^{-2}$
0.98	1	$0.89622 - 0.12214i$	$0.93152 - 0.12406i$	$3.94 \times 10^{-2}, 1.57 \times 10^{-2}$
0.98	2	$0.89358 - 0.20244i$	$0.88668 - 0.25850i$	$7.72 \times 10^{-3}, 2.77 \times 10^{-1}$

IV. CONCLUSIONS

The chances of a multi-mode detection by either Earth- or space-based gravitational wave detectors will depend on the relative amplitude of those modes. Knowing in advance which modes should be excited under a realistic binary merger would reduce the dimensionality of the template bank needed to perform matched filtering on ringdown waveforms. An answer that numerical relativity might provide is precisely which modes are likely to be dominant. This involves predicting the relative amplitudes of different pairs of modes under a variety of scenarios. In this paper we have taken a first step towards understanding the issues involved in such a prediction.

We first presented a systematic way of extracting QNMs from a given signal. Our procedure has a number of built in self-consistency checks, to make sure that when we keep adding modes to our fit we are fitting a true signal and not numerical noise. One of these self-consistency checks is to make sure that we extract the correct quasinormal frequency of each mode within a certain accuracy. If the data being analyzed comes from a numerical simulation,

Table V: Absolute and relative amplitudes as a function of the black hole spin and angular dependence of the perturbations, as predicted by perturbative calculations and as extracted from our numerical evolutions. The amplitudes are given for the wave expressed in Boyer Lindquist coordinates (see appendix A for details) and are multiplied by a factor of r/r_0 to get them in an observer independent form. The last column presents the relative difference between perturbative and numerical results for relative amplitudes. In the corotating case we also extract the amplitude of the first overtone. The differences in the relative amplitudes are considerably smaller when we look at corotating and counterrotating modes, compared to the case of fundamental mode and first overtone with the same angular dependence. This can be explained by the relative magnitude of their damping frequencies, as discussed in Section III B (see also Table IV). This difference becomes less pronounced at very large spins, as expected from the analysis of Section III B.

j	mode			numerical result		perturbation theory		relative difference
	l	m	n	$\mathcal{A}_{\ell mn}$	$\mathcal{A}_{\ell mn}/\mathcal{A}_{220}$	$\mathcal{A}_{\ell mn}$	$\mathcal{A}_{\ell mn}/\mathcal{A}_{220}$	$\mathcal{A}_{\ell mn}/\mathcal{A}_{220}$
0.00	2	2	0	0.211	1.00	0.221	1.00	0.00
0.00	2	2	1	0.316	1.50	0.504	2.28	0.342
0.50	2	2	0	0.201	1.00	0.213	1.00	0.00
0.50	2	-2	0	0.208	1.03	0.228	1.07	0.037
0.50	2	2	1	0.525	2.61	0.768	3.61	0.277
0.90	2	2	0	0.137	1.00	0.148	1.00	0.00
0.90	2	-2	0	0.211	1.54	0.246	1.66	0.072
0.90	2	2	1	0.533	3.89	0.98	6.62	0.412
0.98	2	2	0	0.0833	1.00	0.068	1.00	0.00
0.98	2	-2	0	0.263	3.16	0.257	3.78	0.164
0.98	2	2	1	0.634	7.61	0.416	6.12	0.243

consistent frequencies can be used to monitor the accuracy of the code. If the data is experimental, consistency of the frequencies allows for a test of the no hair conjecture. In more detail: during our fitting procedure we first fit for the dominant mode(s), look at the residual (defined as the difference between our original signal and the fit), make sure that it has a consistent quasinormal ringing behavior and only then fit for the next set of modes, repeating the procedure as long as it makes sense to do so. By following this procedure we have hardly been able to go beyond the first few dominant modes, and this was only possible in very special cases. We expect this to happen with most numerical simulations.

We addressed in some detail the so-called *time-shift problem*. In essence, this is the fact that the quasinormal amplitudes depend exponentially on the quasinormal ringing excitation time, which is not defined unambiguously (not even in the continuum). Furthermore, examining actual values of quasinormal frequencies we have seen that this exponential dependence is an important factor to take into account in practice. To (partially) get rid of this exponential dependence we propose to look at relative amplitudes: choosing pairs of modes whose damping frequency is as close as possible, we can partially cancel each others exponential dependence. We analyzed in detail the exponential dependence of different pairs of modes as a function of the black hole spin. In particular, we found that the *time-shift problem* becomes more important as one increases the spin. For modes with the same value of ℓ , for example, the problem is not very relevant for spins $j \lesssim 0.5$. On the other hand, an accurate extraction of the relative amplitude between the fundamental mode and the first overtone only seems feasible for very high spins and $m > 0$.

Keeping this in mind, we first extracted the fundamental quasinormal frequencies for different values of spin, ranging from $j = 0$ to a rapidly rotating black hole with $j = 0.98$. Even using modest resolutions our frequencies agree with those obtained from perturbation theory within one part in 10^5 to one part in 10^2 , depending on the black hole spin, location of the observer and angular dependence. To our knowledge this is the first time that quasinormal frequencies for scalar perturbations of Kerr, as predicted by perturbation theory, have been verified by numerical evolutions of the field equations.

Next we analyzed in detail the relative amplitude of corotating and counterrotating fundamental modes, as a function of the width of the initial perturbation and the black hole spin, being able to quantify (within the limitations imposed by the *time-shift problem*) under what conditions the asymptotic approximation of Ref. [16] is valid. In particular, we were able to verify the widths of the initial perturbation corresponding to the maximal QNM excitation. Finally, we studied the excitation of overtones. We found that, according to expectations from perturbation theory [16], they get significantly excited for corotating modes and very high spins. In this particular case we were able to extract the complex QNM frequency for the fundamental mode and the first two overtones, with a difference with respect to the predicted values by perturbation theory of the order of a tenth of a percent to ten percent, depending on the mode

and the black hole spin. We expect the techniques and results of this paper to be general enough to be useful for future work on ringdown waveforms.

Acknowledgments

This research was supported in part by NSF grant PHY 05-05761, NASA grant NAG5-1430, and the National Center for Supercomputer Applications grant MCA02N014 to Louisiana State University, and by NSF grant PHY 03-53180 and NASA Grant NNG06GI60 to Washington University. It also employed the resources of the Center for Computation and Technology at Louisiana State University, which is supported by funding from the Louisiana legislature's Information Technology Initiative. We are particularly grateful to Vitor Cardoso for many helpful suggestions and discussions. M. Tiglio thanks S. Teukolsky for hospitality at Cornell University, where part of this work was done. We thank L. Lehner for helpful comments on the manuscript. Our numerical calculations used the Cactus framework [23, 24] with a number of locally developed thorns, the LAPACK [36] and BLAS [37] libraries from the Netlib Repository [38], and the LAM [39, 40, 41] and MPICH [42, 43, 44] MPI [45] implementations.

Appendix A: CHANGE OF COORDINATES AND INITIAL DATA

To compare the numerical results with predictions from perturbation theory we must switch from the usual Boyer-Lindquist coordinates (as used, for example, in [16]) to the Kerr-Schild coordinates used in our code. We denote by (r_*, t) the Boyer-Lindquist radial tortoise coordinate and time, and by (\bar{r}, \bar{t}) the Kerr-Schild coordinates. The transformation we need is given by

$$t(\bar{t}, \bar{r}) = \bar{t} - \Omega(\bar{r}) + \tilde{t}, \quad (\text{A1})$$

$$r_*(\bar{r}) = \bar{r} + \Omega(\bar{r}), \quad (\text{A2})$$

with the definitions

$$\Omega(r) = \frac{2Mr_+}{r_+ - r_-} \ln\left(\frac{r - r_+}{2M}\right) - \frac{2Mr_-}{r_+ - r_-} \ln\left(\frac{r - r_-}{2M}\right), \quad (\text{A3})$$

$$r_+ = M + \sqrt{M^2 - a^2}, \quad (\text{A4})$$

$$r_- = M - \sqrt{M^2 - a^2}. \quad (\text{A5})$$

$$(\text{A6})$$

The reference time \tilde{t} can in principle be freely chosen and is used to define where $t(\bar{r}, \bar{t})$ crosses zero. We fix it by the condition that in both coordinate systems the initial pulse is at the same physical distance from the black hole, i.e. $t(\bar{t} = 0, \bar{r} = \bar{r}_0) = 0$:

$$\tilde{t} = \Omega(\bar{r}_0). \quad (\text{A7})$$

The location of the initial pulse in these coordinates becomes

$$r_0 = \bar{r}_0 + \Omega(\bar{r}_0). \quad (\text{A8})$$

For consistency, the value of σ has to be adjusted to tortoise coordinates. As a rough approximation we set

$$\sigma = \frac{1}{2} [r_*(\bar{r} + \bar{\sigma}) - r_*(\bar{r} - \bar{\sigma})]. \quad (\text{A9})$$

From equations 16 and 25 we read of the exponential decay of each modes amplitude in Boyer-Lindquist coordinates and then substitute them by the Kerr-Schild coordinates. We choose $t_0 = r_* + r_0$.

$$\mathcal{A}_{\ell mn} e^{t - r_* - r_0} = \mathcal{A}_{\ell mn} e^{-2\Omega(\bar{r})\mathcal{I}(\omega_{\ell mn})} e^{\bar{t} - \bar{r} - \bar{r}_0} \equiv \bar{\mathcal{A}}_{\ell mn} e^{\bar{t} - \bar{r} - \bar{r}_0} \quad (\text{A10})$$

This equation relates the amplitudes as seen in Boyer-Lindquist coordinates $\mathcal{A}_{\ell mn}$ with the ones found in the simulations that were done in Kerr-Schild coordinates $\bar{\mathcal{A}}_{\ell mn}$.

[1] J. A. H. Futterman, F. A. Handler, and R. A. Matzner, *Scattering from black holes* (Cambridge University Press, Cambridge, England, 1988).

- [2] C. V. Vishveshwara, *Scattering of gravitational radiation by a Schwarzschild black-hole*, Nature **227**, 936 (1970).
- [3] W. H. Press, *Long wave trains of gravitational waves from a vibrating black hole*, Astrophys. J. **170**, L105 (1971).
- [4] R. Price, *Nonspherical perturbations of relativistic gravitational collapse. I. Scalar and gravitational perturbations*, Phys. Rev. D **5**, 2419 (1972).
- [5] E. Berti and K. D. Kokkotas, *Quasinormal modes of Kerr–Newman black holes: Coupling of electromagnetic and gravitational perturbations*, Phys. Rev. D **71**, 124008 (2005), gr-qc/0502065.
- [6] F. Echeverría, *Gravitational-wave measurements of mass and angular momentum of a black hole*, Phys. Rev. D **40**, 3194 (1989).
- [7] L. S. Finn, *Detection, measurement, and gravitational radiation*, Phys. Rev. D **46**, 5236 (1992).
- [8] E. Berti, V. Cardoso, and C. M. Will, *On gravitational-wave spectroscopy of massive black holes with the space interferometer LISA*, Phys. Rev. D **73**, 064030 (2006), gr-qc/0512160.
- [9] O. Dreyer, B. Kelly, B. Krishnan, L. S. Finn, D. Garrison, and R. Lopez-Aleman, *Black hole spectroscopy: Testing general relativity through gravitational wave observations*, Class. Quantum Grav. **21**, 787 (2004), gr-qc/0309007.
- [10] E. E. Flanagan and S. Hughes, *Measuring gravitational waves from binary black hole coalescences. I. Signal to noise for inspiral, merger, and ringdown*, Phys. Rev. D **57**, 4535 (1998).
- [11] E. Berti, A. Buonanno, and C. M. Will, *Estimating spinning binary parameters and testing alternative theories of gravity with LISA*, Phys. Rev. D **71**, 084025 (2005), gr-qc/0411129.
- [12] M. Luna and A. M. Sintes, *Parameter estimation of compact binaries using the inspiral and ringdown waveforms* (2006), gr-qc/0601072.
- [13] K. D. Kokkotas and B. G. Schmidt, *Quasi-normal modes of stars and black holes*, Living Rev. Relativity **2**, 2 (1999), URL <http://www.livingreviews.org/lrr-1999-2>.
- [14] H.-P. Nollert, *Quasinormal modes: The characteristic “sound” of black holes and neutron stars*, Class. Quantum Grav. **16**, R159 (1999).
- [15] E. Berti, *Black hole quasinormal modes: Hints of quantum gravity?* (2004), gr-qc/0411025.
- [16] E. Berti and V. Cardoso, *Quasinormal ringing of Kerr black holes. I: The excitation factors* (2006), gr-qc/0605118.
- [17] E. Berti, V. Cardoso, and C. M. Will, *Considerations on the excitation of black hole quasinormal modes* (2006), gr-qc/0601077.
- [18] E. Schnetter, P. Diener, N. Dorband, and M. Tiglio, *A multi-block infrastructure for three-dimensional time-dependent numerical relativity*, Class. Quantum Grav. **23**, S553 (2006), gr-qc/0602104, URL <http://stacks.iop.org/CQG/23/S553>.
- [19] L. Lehner, O. Reula, and M. Tiglio, *Multi-block simulations in general relativity: high order discretizations, numerical stability, and applications*, Class. Quantum Grav. **22** (2005), gr-qc/0507004.
- [20] P. Diener, E. N. Dorband, E. Schnetter, and M. Tiglio, *New, efficient, and accurate high order derivative and dissipation operators satisfying summation by parts, and applications in three-dimensional multi-block evolutions* (2005), gr-qc/0512001.
- [21] E. Schnetter, S. H. Hawley, and I. Hawke, *Evolutions in 3D numerical relativity using fixed mesh refinement*, Class. Quantum Grav. **21**, 1465 (2004), gr-qc/0310042.
- [22] Mesh Refinement with Carpet, URL <http://www.carpetcode.org/>.
- [23] T. Goodale, G. Allen, G. Lanfermann, J. Massó, T. Radke, E. Seidel, and J. Shalf, *The Cactus framework and toolkit: Design and applications*, in *Vector and Parallel Processing – VECPAR’2002, 5th International Conference, Lecture Notes in Computer Science* (Springer, Berlin, 2003), URL <http://www.cactuscode.org/Publications/>.
- [24] Cactus Computational Toolkit home page, URL <http://www.cactuscode.org/>.
- [25] W. Krivan, P. Laguna, and P. Papadopoulos, *Dynamics of scalar fields in the background of rotating black holes*, Phys. Rev. D **54**, 4728 (1996).
- [26] W. Krivan, P. Laguna, P. Papadopoulos, and N. Andersson, *Dynamics of perturbations of rotating black holes*, Phys. Rev. D **56**, 3395 (1997).
- [27] M. Saijo, H. Shinkai, and K. Maeda, *Gravitational waves in Brans-Dicke theory: Analysis by test particles around Kerr black hole*, Phys. Rev. D **56**, 785 (1997), gr-qc/9701001.
- [28] L. Lehner, D. Neilsen, O. Reula, and M. Tiglio, *The discrete energy method in numerical relativity: Towards long-term stability*, Class. Quantum Grav. **21**, 5819 (2004), gr-qc/0406116.
- [29] E. Leaver, *An analytic representation for the quasi-normal modes of Kerr black holes*, Proc. R. Soc. London, Ser. A **402**, 285 (1985).
- [30] E. Berti, V. Cardoso, and M. Casals, *Eigenvalues and eigenfunctions of spin-weighted spheroidal harmonics in four and higher dimensions*, Phys. Rev. D **73**, 024013 (2006).
- [31] W. H. Press and S. A. Teukolsky, *Perturbations of a rotating black hole. II. Dynamical stability of the Kerr metric*, Astrophys. J. **185**, 649 (1973).
- [32] Y. Zlochower, R. Gómez, S. Husa, L. Lehner, and J. Winicour, *Mode coupling in the nonlinear response of black holes*, Phys. Rev. D **68**, 084014 (2003).
- [33] G. Allen, K. Camarda, and E. Seidel, *Evolution of distorted black holes: A perturbative approach* (1998), gr-qc/9806014, submitted to Phys. Rev. D.
- [34] N. Andersson, *Excitation of Schwarzschild black-hole quasinormal modes*, Phys. Rev. D **51**, 353 (1995).
- [35] E. N. Dorband and M. Tiglio (2006), in preparation.
- [36] LAPACK: Linear Algebra Package, URL <http://www.netlib.org/lapack/>.
- [37] BLAS: Basic Linear Algebra Subroutines, URL <http://www.netlib.org/blas/>.
- [38] Netlib Repository, URL <http://www.netlib.org/>.
- [39] G. Burns, R. Daoud, and J. Vaigl, *LAM: An Open Cluster Environment for MPI*, in *Proceedings of Supercomputing*

- Symposium* (1994), pp. 379–386, URL <http://www.lam-mpi.org/download/files/lam-papers.tar.gz>.
- [40] J. M. Squyres and A. Lumsdaine, *A Component Architecture for LAM/MPI*, in *Proceedings, 10th European PVM/MPI Users' Group Meeting* (Springer-Verlag, Venice, Italy, 2003), no. 2840 in Lecture Notes in Computer Science, pp. 379–387.
 - [41] LAM: LAM/MPI Parallel Computing, URL <http://www.lam-mpi.org/>.
 - [42] W. Gropp, E. Lusk, N. Doss, and A. Skjellum, *A high-performance, portable implementation of the MPI message passing interface standard*, *Parallel Computing* **22**, 789 (1996).
 - [43] W. D. Gropp and E. Lusk, *User's Guide for mpich, a Portable Implementation of MPI*, Mathematics and Computer Science Division, Argonne National Laboratory (1996), ANL-96/6.
 - [44] MPICH: ANL/MSU MPI implementation, URL <http://www-unix.mcs.anl.gov/mpi/mpich/>.
 - [45] MPI: Message Passing Interface Forum, URL <http://www.mpi-forum.org/>.